

## Research Article

# Dataflow-Based Mapping of Computer Vision Algorithms onto FPGAs

Mainak Sen,<sup>1</sup> Ivan Corretjer,<sup>1</sup> Fiorella Haim,<sup>1</sup> Sankalita Saha,<sup>1</sup> Jason Schlessman,<sup>2</sup> Tiehan Lv,<sup>2</sup> Shuvra S. Bhattacharyya,<sup>1</sup> and Wayne Wolf<sup>2</sup>

<sup>1</sup>Department of Electrical and Computer Engineering, University of Maryland, College Park, MD 20742, USA

<sup>2</sup>Department of Electrical Engineering, Princeton University, Princeton, NJ 08544, USA

Received 1 May 2006; Revised 8 October 2006; Accepted 9 October 2006

Recommended by Moshe Ben-Ezra

We develop a design methodology for mapping computer vision algorithms onto an FPGA through the use of coarse-grain reconfigurable dataflow graphs as a representation to guide the designer. We first describe a new dataflow modeling technique called homogeneous parameterized dataflow (HPDF), which effectively captures the structure of an important class of computer vision applications. This form of dynamic dataflow takes advantage of the property that in a large number of image processing applications, data production and consumption rates can vary, but are equal across dataflow graph edges for any particular application iteration. After motivating and defining the HPDF model of computation, we develop an HPDF-based design methodology that offers useful properties in terms of verifying correctness and exposing performance-enhancing transformations; we discuss and address various challenges in efficiently mapping an HPDF-based application representation into target-specific HDL code; and we present experimental results pertaining to the mapping of a gesture recognition application onto the Xilinx Virtex II FPGA.

Copyright © 2007 Mainak Sen et al. This is an open access article distributed under the Creative Commons Attribution License, which permits unrestricted use, distribution, and reproduction in any medium, provided the original work is properly cited.

## 1. BACKGROUND AND MOTIVATION

Computer vision methods based on real-time video analysis form a challenging and increasingly important domain for embedded system design. Due to their data-intensive nature, hardware implementations for real-time video are often more desirable than corresponding software implementations despite the relatively longer and more complicated development processes associated with hardware implementation. The approach that we pursue in this paper is based on direct representation by the designer of application concurrency using dataflow principles. Dataflow provides an application modeling paradigm that is well suited to parallel processing (and to other forms of implementation streamlining) for digital signal processing (DSP) systems [1]. Dataflow is effective in many domains of DSP, including digital communications, radar, and video processing.

In this paper, we use dataflow as a conceptual tool to be applied by the designer rather than as the core of an automated translation engine for generating HDL code. This combination of a domain-specific model of computation, and its use as a conceptual design tool rather than an

automated one allows great flexibility in streamlining higher level steps in the design process for a particular application.

As an important front-end step in exploiting this flexibility, we employ HPDF (homogeneous parameterized dataflow) [2] semantics to represent the behavior of the target gesture recognition system. HPDF is a restricted form of dynamic dataflow and is not supported directly by any existing synthesis tools. However, an HPDF-based modeling approach captures the high-level behavior of our gesture recognition application in a manner that is highly effective for design verification and efficient implementation. As our work in this paper demonstrates, the HPDF-based representation is useful to the designer in structuring the design process and bridging the layers of algorithm and architecture, while HDL synthesis tools play the complementary role of bridging the architecture and the target platform.

## 2. RELATED WORK

Modeling computer vision applications using dataflow graphs can lead to useful formal properties, such as bounded memory requirements, and efficient synthesis solutions [3]. The synchronous dataflow (SDF) model, for example, has

particularly strong compile time predictability properties [4]. However, this model is highly restrictive and cannot handle data-dependent execution of dataflow graph vertices (*actors*). A cyclostatic dataflow (CSDF) [5] graph can accommodate multiphase actors but still does not permit data dependent production or consumption patterns. The token flow model [6] provides for dynamic actors where the number of data values (*tokens*) transferred across a graph edge may depend on the run-time value of a token that is received at a “control port” of an incident actor. A metamodeling technique called parameterized dataflow [7] (PDF) has been proposed in which dynamic dataflow capabilities are formulated in terms of run-time reconfiguration of actor and edge parameters.

A number of studies have been undertaken in recent years on the design and implementation of multimedia applications on FPGAs using other formal or systematic approaches. Streams-C [8] provides compiler technology that maps high-level *parallel C* language descriptions into circuit-level netlists targeted to FPGAs. To use Streams-C effectively, the programmer needs to have some application-specific hardware mapping expertise as well as expertise in parallel programming under the communicating sequential processes (CSP) model of computation [9]. Streams-C consists of a small number of libraries and intrinsic functions added to a subset of C that the user must use to derive synthesizable HDL code.

Handel-C [10] represents another important effort towards developing a hardware oriented C language. Handel-C is based on a subset of the ANSI C standard along with extensions that support a synchronous parallel mode of operation. This language also conforms to the CSP model.

Match [11], or AccelFPGA as it is called now, generates VHDL or Verilog from an algorithm coded in MATLAB, a programming language that is widely used for prototyping image and video processing algorithms. AccelFPGA has various compiler directives that the designer can use to explore the design space for optimized hardware implementation. Loop unrolling, pipelining, and user-defined memory mapping are examples of implementation aspects that can be coordinated through AccelFPGA directives.

Compaan [12] is another design tool for translating MATLAB programs into HDL for FPGA implementation. Compaan performs its translation through an intermediate representation that is based on the Kahn process network model of computation [13].

Rather than adapting a sequential programming language for hardware design, as the above-mentioned approaches do, our approach is based on concurrency exposed by the designer in representing the algorithm as a dataflow model. This is a useful approach for signal processing because the structure of signal processing applications in terms of its coarse-grain components (e.g., FIR filters, IIR filters, and FFT computations) often translates intuitively into concurrent specifications based on dataflow principles.

### 3. DYNAMIC DATAFLOW MODELING

In this section, we present a brief background on parameterized dataflow (PDF), and parameterized synchronous dataflow (PSDF), and we formulate a new dataflow metamodeling technique called homogeneous parameterized dataflow (HPDF). Like parameterized dataflow, HPDF is a metamodeling technique that can be applied to any underlying dataflow model of computation  $M$  that has a well-defined notion of a *graph iteration*. When a model  $M$  is used in conjunction with HPDF or parameterized dataflow, it is called the *base model* to which the metamodeling approach is applied.

#### 3.1. Parameterized dataflow

Parameterized dataflow [7] increases the expressive power of the underlying base model by providing for run-time reconfigurability of actor and edge parameters in a certain structured way. When parameterized dataflow is applied to SDF as the base model, the resulting model of computation is called parameterized synchronous dataflow (PSDF). The PSDF model can be viewed as an augmentation of SDF that incorporates run-time reconfiguration of parameters for actors, subsystems, and edges.

An actor  $A$  in PSDF is characterized by a set of parameters ( $params(A)$ ) that control the actor’s functionality, including possibly its dataflow behavior. Each parameter is either assigned a value from a set of viable values or left unspecified. These unspecified parameters are assigned values at run time through a disciplined run-time reconfiguration mechanism. Techniques have been developed to execute PSDF graphs efficiently through carefully constructed quasistatic schedules [7].

PSDF specifications are built up in a modular way in terms of hierarchical subsystems. Every subsystem is in general composed of three subgraphs, called the *init*, *subinit* and *body* graphs. New parameter values to use during run-time reconfiguration are generally computed in the *init* and *subinit* graphs, and the values are propagated to the *body* graph, which represents the computational core of the associated PSDF subsystem. The *init* graph is invoked at the beginning of each invocation of the (hierarchical) parent graph and the *subinit* graph is invoked at the beginning of each invocation of the associated subsystem followed by the *body* graph. Intuitively, reconfiguration of a *body* graph by the corresponding *init* graph occurs less frequently but is more flexible compared to reconfiguration by the *subinit* graph [7].

#### 3.2. Homogeneous parameterized dataflow

In this section, we develop the HPDF model which, like parameterized dataflow, is a metamodeling technique in that it can be applied to different dataflow base models. In this section, we present the characteristics of the actors, edges, and delay buffers in an HPDF graph.

An HPDF subsystem is homogeneous in two ways. First, unlike general SDF graphs and other multirate models, the top level actors in an HPDF subsystem execute at the same rate. Second, unlike the hierarchically oriented parameterized dataflow semantics, reconfiguration across subsystems can be achieved without introducing hierarchy (i.e., reconfiguration across actors that are at the same level of the modeling hierarchy). Some dynamic applications are naturally nonhierarchical (as we show in Section 5), and this kind of behavior can be modeled using HPDF without imposing “artificial” hierarchical structures that a parameterized dataflow representation would entail. At the same time, hierarchy can be used within the HPDF framework when it is desired.

HPDF is a metamodeling technique. Composite actors in an HPDF model can be refined using any dataflow modeling semantics that provide a well-defined notion of subsystem iteration. For example, the composite HPDF actor might have SDF, CSDF, PSDF or multidimensional SDF [14] actors as its constituent actors.

As with many other dataflow models, such as SDF and CSDF, an HPDF  $e$  edge can have a nonnegative integer delay  $\delta(e)$  on it. This delay gives the number of initial data samples (tokens) on the edge. The stream of tokens that is passed across an edge needs markers of some kind to indicate the “packets” that correspond to each iteration of the producing and consuming actors. An end-of-packet marker is used for this purpose in our implementation.

Interface actors in HPDF can produce and consume arbitrary amounts of data, while the internal connections must, for fixed parameter values, obey the constraints imposed by the base model. An HPDF source actor in general has access to a variable number of tokens at its inputs, but it obeys the semantics of the associated base model on its output. Similarly, an HPDF sink actor obeys the semantics of its base model at the input but can produce a variable number of tokens on its output. HPDF source and sink actors can be used at subsystem interfaces to connect hierarchically to other forms of dataflow.

### 3.3. Comparison of HPDF and PSDF

While HPDF employs parameterized actors and subsystems like PSDF, there are several distinguishing features of HPDF in relation to PSDF. For example, unlike PSDF, HPDF always executes in bounded memory whenever the component models execute in bounded memory. In contrast, some PSDF systems do not execute in bounded memory, and in general, a combination of static and run-time checks is needed to ensure bounded memory operation for PSDF [7].

Also, as described in Section 3.2, we do not have to introduce hierarchy in HPDF to account for dynamic behavior of actors. For example, suppose that a dynamic source actor  $A$  produces  $n$  tokens that are consumed by the dynamic sink actor  $B$ . In PSDF, we need to have  $A$  and  $B$  in different subsystems; the body of  $A$  would set the parameter  $n$ , which will be a known quantity at that time, in the subunit of  $B$  (see Section 5.1 for a more detailed example). This hierarchy

can be avoided in HPDF as we assume that data is produced and consumed in same-sized blocks. As we will describe further in Section 5, this simple form of dynamicity has many applications in signal processing algorithms. It therefore deserves explicit efficient support as provided by HPDF.

In summary, compared to PSDF, HPDF provides for simpler (nonhierarchical) parameter reconfiguration, and for more powerful static analysis. In exchange for these features, HPDF is significantly more narrow in the scope of applications that it is suitable for. Intuitively, a parameterized multirate application cannot be modeled using HPDF. However, as we motivate in this paper, HPDF is suitable for an important class of computer vision applications, and therefore it is a useful modeling approach to consider when developing embedded hardware and software for computer visions systems.

## 4. GESTURE RECOGNITION APPLICATION

As a consequence of continually improving CMOS technology, it is now possible to develop “smart camera” systems that not only capture images, but also process image frames in sophisticated ways to extract “meaning” from video streams. One important application of smart cameras is gesture recognition from video streams of human subjects. In the gesture recognition algorithm discussed in [15], for each image captured, real-time image processing is performed to identify and track human gestures. As the flow of images is increased, a higher level of reasoning about human gestures becomes possible. This type of processing occurs inside the smart camera system using advanced very large scale integration (VLSI) circuits for both low-level and high-level processing of the information contained in the images. Figure 1 gives an overview of the smart camera gesture recognition algorithm.

The functional blocks of particular interest in this paper are the low-level processing components *Region*, *Contour*, *Ellipse*, and *Match* (within the dotted rectangle in Figure 1). Each of these blocks operate at the pixel level to identify and classify human body parts in the image, and are thus good candidates for implementation on a high-performance field-programmable gate array (FPGA).

The computational core of the block diagram in Figure 1 can be converted from being an intuitive flow diagram to a precise behavioral representation through integration of HPDF modeling concepts. This exposes significant patterns of parallelism and of predictability, which together with application specific optimizations help us to map the application efficiently into hardware.

The front-end processing is performed by Region extraction (*Region*), which accepts a set of three images as inputs (we will refer to this set as an image group from now on). The input images constituting the image group are in the  $Y C_r C_b$  color space in which  $Y$  represents the intensity and  $C_r, C_b$  represents the chrominance components of the image. In the current application input, chrominance components are downsampled by a factor of two. Thus, the three

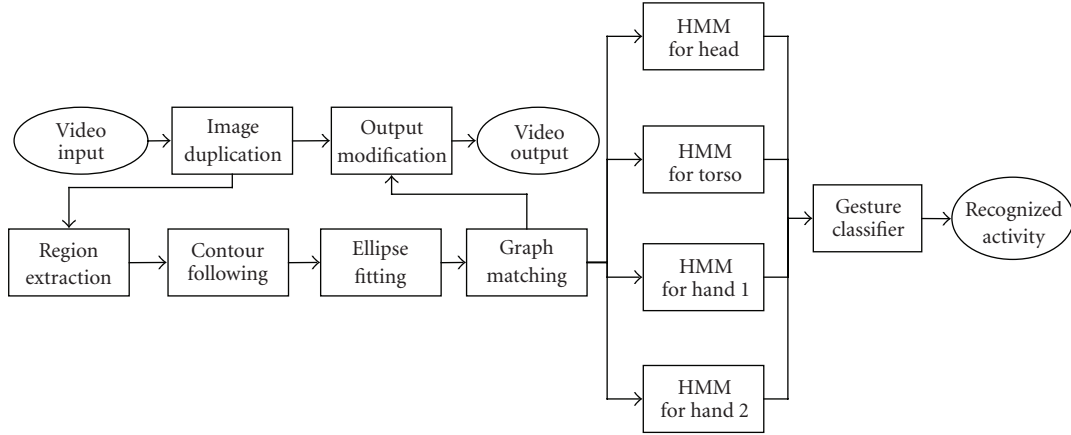


FIGURE 1: Block level representation of the smart camera algorithm [15].

images in the image group sent as input to Region extraction are

- (i) the  $Y$  component (Image 1 in Figure 5);
- (ii) the background (Image 2 in Figure 5); and
- (iii) the downsampled  $C_r, C_b$  components together (Image 3 in Figure 5).

The image with background regions is used in processing the other two images, which have foreground information as well. In one of the foreground images, the Region block marks areas that are of human-skin tones, and in the other, it marks areas that are of nonskin tone. Each of these sets of three images is independent of the next set of three, revealing image-level parallelism.

Additionally, modeling the algorithm with finer granularity (Section 5.3) exposes that the set of three pixels from the corresponding coordinates in the images within an image group are independent of any other set of pixels, leading to pixel-level parallelism. This has been verified by simulating the model for correct behavior. Furthermore, the operations performed are of similar complexity, suggesting that a synchronous pipeline implementation with little idle time between stages is possible.

After separating foreground regions into two images, each containing only skin and nonskin tone regions respectively, the next processing stage that occurs is contour following (Contour). Here, each image is scanned linearly pixel-by-pixel until one of the regions marked in the Region stage is encountered. For all regions in both images (i.e., regardless of skin or nonskin tone), the contour algorithm traces out the periphery of each region, and stores the  $(x, y)$  locations of the boundary pixels. In this way, the boundary pixels making up each region are grouped together in a list and passed to the next stage.

The ellipse fitting (Ellipse) functional block processes each of the contours of interest and characterizes their shapes through an ellipse-fitting algorithm. The process of ellipse fitting is imperfect and allows for tolerance in the deformations caused during image capture (such as objects obscuring

portions of the image). At this stage, each contour is processed independently of the others, revealing contour-level parallelism.

Finally, the graph matching (Match) functional block waits until each contour is characterized by an ellipse before beginning its processing. The ellipses are then classified into head, torso, or hand regions based on several factors. The first stage attempts to identify the head ellipse, which allows the algorithm to gain a sense of where the other body parts should be located relative to the head. After classifying the head ellipse, the algorithm proceeds to find the torso ellipse. This is done by comparing the relative sizes and locations of ellipses adjacent to the head ellipse, and using the fact that the torso is usually larger by some proportion than other regions and that it is within the vicinity of the head. The conditions and values used to make these determinations are part of a piecewise quadratic Bayesian classifier that only requires the six characteristic parameters from each ellipse in the image [15].

## 5. MODELING THE GESTURE RECOGNITION ALGORITHM

In this section, we model the gesture recognition algorithm using both PSDF and HPDF, and then show some application specific optimizations that are aided by the HPDF representation.

### 5.1. Modeling with PSDF

As mentioned in Section 3.1, PSDF imposes a hierarchy discipline. The gesture recognition algorithm is modeled using PSDF in Figure 2. At the uppermost level, the Ges-Recog. subsystem has empty init and subinit graphs, and GesRecog.body is the body graph for the subsystem that has two hierarchical subsystems— $H_E$  and  $H_M$ . The subsystems  $H_E$  and  $H_M$  in turn each have two input edges. On one of these edges, one token is consumed; this token provides the number of tokens (e.g., the value of  $p_2$  on the edge between

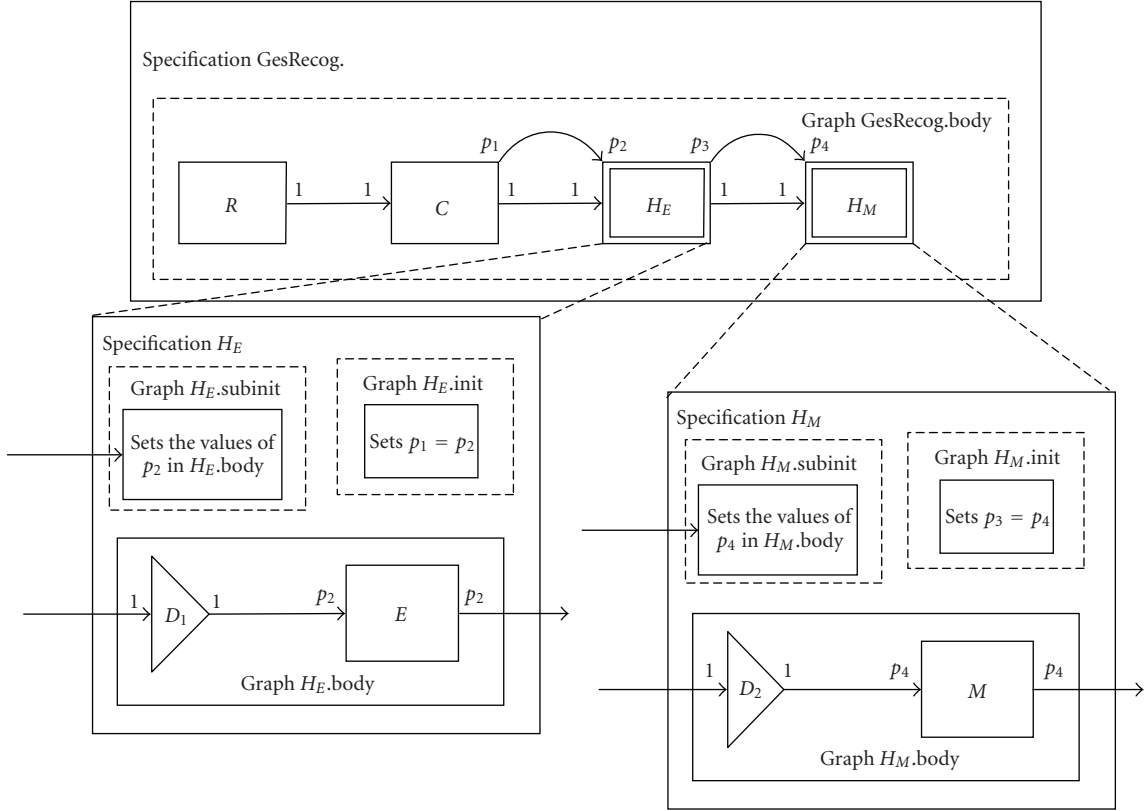


FIGURE 2: PSDF modeling of the Gesture Recognition application.

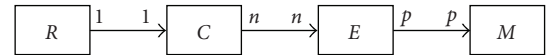
$C$  and  $H_E$  in Figure 2) that is to be consumed on the other edge, which is edge that contains the actual tokens that are to be processed.

The body graph of  $H_E$  has the actor  $E$  embedded inside.  $H_E \cdot \text{init}$ , which is called once per iteration of the GesRecog. subsystem, has one actor in the graph. This actor sets the parameters  $p_1 = p_2$  in the body graph. The  $H_E \cdot \text{subinit}$  graph has one actor, which sets in  $p_2$  in  $H_E \cdot \text{body}$  with the value sent by the actor  $C \cdot D_1$  is a dummy “gain” actor required so that the schedule in the body graph is  $p_2 D_1 E$  to accommodate for  $p_2$  tokens as input to  $E$ . Analogous behavior is seen in  $H_M \cdot \text{init}$ ,  $H_M \cdot \text{subinit}$ , and  $H_M \cdot \text{body}$ .

### 5.2. Modeling with HPDF over SDF

We prototyped an HPDF-based model of the gesture recognition algorithm in Ptolemy II [16], a widely used software tool for experimenting with new models of computation and integrating different models of computation. Here, we applied SDF as the base model to which the HPDF metamodel is applied. Our prototype was developed to validate our HPDF representation of the application, simulate its functional correctness, and provide a reference to guide the mapping of the application into hardware.

In the top level, the HPDF application representation contains four hierarchical actors (actors that represent

FIGURE 3: HPDF model of the application with parameterized token and consumption rates, where  $R$  is Region,  $C$  is Contour,  $E$  is Ellipse, and  $M$  is Match.

nested subsystems)—Region, Contour, Ellipse, and Match—as shown in Figure 3. The symbols on the edges represent the numbers of data values produced and consumed on each execution of the actor. Here  $n$  and  $p$  are parameterized data transfer rates that are not known statically. Furthermore, the rates can vary during execution subject to certain technical restrictions that are imposed by the HPDF model, as described in Section 3.2.

### 5.3. Modeling with HPDF over CSDF

We have further refined our model for the gesture recognition algorithm using CSDF [17] as the base model for HPDF. Figure 4 shows that Region can be represented as a CSDF subsystem with  $s$  phases, where  $s$  is the number of pixels in one input frame, and Region can work on a per-pixel basis (pixel-level parallelism). On the other hand, Figure 4 suggests that Contour needs the whole image frame to start execution.

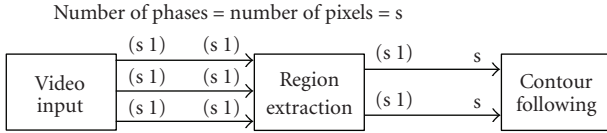


FIGURE 4: Model of the static part of the system.

#### 5.4. Modeling the actors

By examining the HPDF graph in conjunction with the intra-actor specifications (the actors were specified using Java in our Ptolemy II prototype), we derived a more detailed representation as a major step in our hardware mapping process. This representation is illustrated across Figures 5 and 6, which are lower-level dataflow representations of Region and Contour, respectively. Here, as with other dataflow diagrams, the round nodes ( $A$ ,  $B$ ,  $C$ ,  $D$ , and  $E$ ) represent computations, and the edges represent unidirectional data communication.

Figures 5 and 6 are created by hand while mapping Region and Contour to dataflow structures, and the actors  $A$  through  $E$  are each implemented in a few lines of Java code. These are more refined dataflow representations of the actors in the original HPDF representation. This kind of dataflow mapping from the corresponding application is a manual process, and depends on the expertise of the designer as well as the suitability of the form of dataflow that is being applied. In this particular case, the actors  $A$  to  $E$  represent the following operations ( $Image I$  here represents one pixel from the corresponding Image  $I$  and the algorithm runs for all the pixels in those images,  $thold_i$  represents threshold values described in the algorithm):

- (i)  $A$  represents  $abs(Image 1 - Image 2)$ ;
- (ii)  $B$  represents  $if(Image 3 > thold_1)$ ;
- (iii)  $C$  represents  $if(((A) > thold_2) \wedge (thold_3 > Image 1 > thold_4))$ ;
- (iv)  $D$  represents  $if(A > thold_5)$ ; and
- (v)  $E$  represents  $\overline{CD} + \overline{CB}$ .

The square nodes in Figure 5 represent image buffers or memory, and the diamond-shaped annotations on edges represent delays. The representation of Figure 5 reveals that even though buffers  $Image 1$  and  $Image 3$  are being read from and written into the reading and writing occur in a mutually noninterfering way. Furthermore, separating the two buffers makes the four-stage pipeline implementation a natural choice.

In Contour (Figure 6), the dotted edges represent *conditional data transfer*. In each such conditional edge, zero or one-data item can be produced by the source actor depending on its input data. More specifically, in Figure 6 there will either be one-data value produced on the edge between  $A$  and  $B$  or on the self-looped edge, and the other edge will have zero-data items produced. The representation of Figure 4 and its data transfer properties motivated us to map the associated functionality into a four-stage self-timed process.

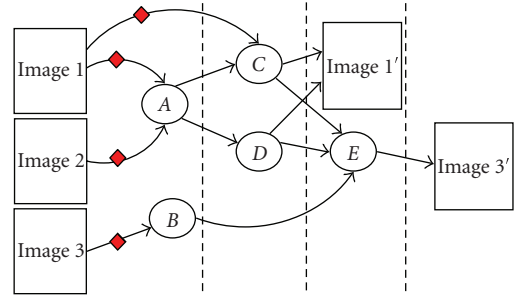


FIGURE 5: Region is shown to be broken into a four-stage pipeline process.

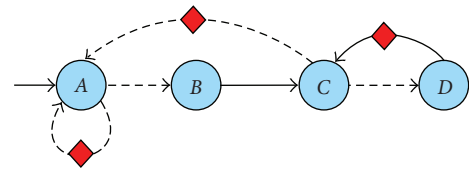


FIGURE 6: Contour is shown to have *conditional edges* and serial execution. This structure is implemented as a four-stage self-timed process.

## 6. FROM THE MODEL TO HARDWARE

Dataflow modeling of an application has been used extensively as an important step for verification, and for performing methodical software synthesis [16]. Hardware synthesis from SDF and closely related representations has also been explored (e.g., see [18–20]). In this paper, we explore the hardware synthesis aspects for class of dynamic dataflow representations that can be modeled using HPDF. Compared to PSDF, HPDF can be more suited to intuitive manual hardware mapping because of its nonhierarchical dynamic dataflow approach. For example, Figure 3 might suggest a power-aware self-timed architecture, where the different hardware modules hibernate and are occasionally awakened by the preceding module in the chain. Alternatively, it can also suggest a pipelined architecture with four stages for high performance. The designer can also suggest multiple instantiations of various modules based on applying principles of data parallelism on the dataflow graph [19]. Such application of data parallelism can systematically increase throughput without violating the dataflow constraints of the application. Hence, an HPDF model can suggest a range of useful architectures for an application, and thus aid the designer significantly in design-space exploration.

In Region, the application level dataflow model (which shows pixel-level parallelism) in conjunction with actor level dataflow (which suggests a pipelined architecture) suggests that the pipeline stages should work on individual pixels and not on the whole frame for maximum throughput. On the other hand for Contour, a self-timed architecture that performs on the whole image was a natural choice.

In addition to dataflow modeling, we also applied some application specific transformations. For example, the Ellipse module utilizes floating-point operations to fit ellipses to the various contours. The original C code implementation uses a moment-based initialization procedure along with trigonometric and square-root calculations. The initialization procedure computes the averages of the selected contour pixel locations and uses these averages to compute the various moments. The total computation cost is

$$5nC_+ + 6nC_- + 3nC_* + 5C_j, \quad (1)$$

where  $n$  is the number of pixels in the contour, and each term  $C_{OP}$  represents the cost of performing operation OP. In an effort to save hardware and reduce complexity, the following transformation was applied to simplify the hardware for calculating averages and moments:

$$mxx = \left( \sum_{i=1}^n \frac{(x_i - \bar{x})^2}{n} \right) \Rightarrow \left( \sum_{i=1}^n \frac{(x_i)^2}{n} - \overline{(x)^2} \right), \quad (2)$$

and similarly for  $mxy$  and  $myy$ . The computational cost after this transformation is

$$5nC_+ + 3nC_* + 9C_j + 3C_- + 3C_*. \quad (3)$$

Comparing this with the expression for the previous version of the algorithm, we observe a savings of  $3nC_-$ , which increases linearly with the number of contour pixels, at the expense of a fixed overhead  $4C_j + 3C_*$ . This amounts to a large overall savings for practical image sizes.

Further optimizations that were performed on the ellipse-fitting implementation included splitting the calculations into separate stages. This allowed for certain values (such as  $nxx$ ,  $myy$ ,  $mxy$ ) to be computed in earlier stages and reused multiple times in later stages to remove unnecessary computations.

The characterization of ellipses in Match is accomplished in a serial manner, in particular, information about previously identified ellipses is used in the characterization of future ellipses. Our functional prototype of the matching process clearly showed this dependency of later stages on previous stages. The hardware implementation that we derived is similar to that of Contour, and employs a six-stage self-timed process to efficiently handle the less predictable communication behavior.

## 7. EXPERIMENTAL SETUP

The target FPGA board chosen for this application is the multimedia and microblaze development board from Xilinx. The board can act as a platform to develop a wide variety of applications such as image processing and ASIC prototyping. It features the XC2V2000 device of the Virtex II family of FPGAs.

Some of the more important features of the board include the following.

- (i) Five external independent 512 K × 36 bit ZBT RAMs.
- (ii) A video encoder-decoder.

- (iii) An audio codec.
- (iv) Support for PAL/NTSC TV input/output.
- (v) On-board ethernet support.
- (vi) An RS-232 port.
- (vii) Two PS-2 serial ports.
- (viii) A JTAG port.
- (ix) A system ACE-controller and compact flash storage device to program the FPGA.

### 7.1. ZBT memory

One of the key features of this board is its set of five fully independent banks of 512 k × 32 ZBT RAM [21] with a maximum clock rate of 130 MHz. These memory devices support a 36-bit data bus, but pinout limitations on the FPGA prevent the use of the four parity bits. The banks operate completely independently of one another, as the control signals, address, data busses, and clock are unique to each bank with no sharing of signals between the banks. The byte write capability is fully supported as it is the burst mode in which the sequence starts with an externally supplied address.

Due to the size of the images, we needed to store them using these external RAMs. A memory controller module was written in Verilog, simulated, synthesized, and downloaded onto the board. We then successfully integrated this module with the Region module.

### 7.2. RS-232

In order to communicate between the host PC and the board, we used the RS-232 protocol. We adapted an RS232 controller core with a wishbone interface [22] and configurable baud rate to write images from the PC to the memory. The board acts as a DCE device; we implemented the physical communication using a straight-through three wire cable (pins 2, 3, and 5) and used the Windows hyperterminal utility to test it. This interface was integrated into the Region and memory controller modules and tested in the board.

Figure 7 illustrates the overall experimental setup, including the interactions between the PC and the multimedia board, and between the board and the HDL modules.

## 8. DESIGN TRADEOFFS AND OPTIMIZATIONS

There were various design decisions made during implementation of the algorithm, some of which were specific to the algorithm at hand. In this section, we explore in more detail the tradeoffs that were present in the important design space associated with memory layout. We also present a step-by-step optimization that we performed on one of the design modules for reducing its resource requirements on the FPGA.

### 8.1. Memory layout tradeoffs

The board memory resources are consumed by the storing of the images. Each of the 5 ZBT RAM banks can store 512 K words that are 32-bits long, for a total storage capacity of 10

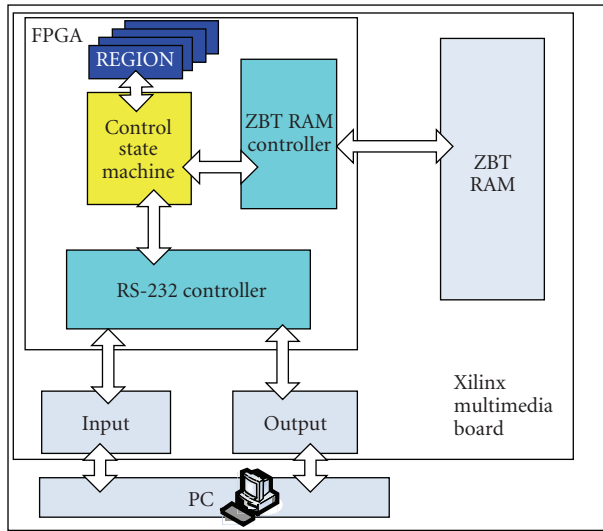


FIGURE 7: The overall setup interactions among various modules of our design and components of the multimedia board.

megabytes. Given that each pixel requires one byte of storage and that there are  $384 \times 240$  pixels per image, 90 kilobytes of memory are required to store each image. The first module, Region, has 3 images as inputs, and 2 images as outputs. These two images are scanned serially in the second module, Contour. The total amount of memory needed for image storing is then 450 kilobytes, less than 5% of the external memory available on board. However, reorganization of the images in the memory can dramatically change the number of memory access cycles performed and the number of banks used. These tradeoffs also affect the total power consumption.

Several strategies are possible for storing the images in the memory. The simplest one (Case 1) would be to store each of the five images in a different memory bank, using 90 K addresses and the first byte of each word. In this way, the 5 images can be accessed in the same clock cycle (Figure 8(a)). However, we can minimize the number of memory banks used by exploiting the identical order in which the reading and writing of the images occurs (Case 2). Thus, we can store the images in only two blocks, using each of the bytes of a memory word for a different image, and still access all the images in the same clock cycle (Figure 8(b)).

On the other hand, a more efficient configuration in order to minimize the number of memory access cycles (Case 3) would be to store each image in a different bank, but using the four bytes of each memory word consecutively (Figure 8(c)). Other configurations are possible, for example, (Case 4) we can have two images per bank, storing 2 pixels of each image in the same word (Figure 8(d)). Table 1 summarizes the number of banks and memory access cycles needed for each of these configurations.

Case 3 appears to be the most efficient memory organization. Here, the time associated with reading and writing of the images is 69120 memory access cycles, and the total

number of memory access cycles is also the lowest, 161280. This reduced number of memory access cycles suggests that power consumption will also be relatively low in this configuration. Figure 8 illustrates all of the cases discussed above.

## 8.2. Floating-point optimizations

Floating-point operations are used throughout the implementation of the Ellipse and Match blocks. The Ellipse block processes the  $(x, y)$  location of every pixel that is along the border of a contour. From these locations, averages, moments, and rotation parameters are derived that characterize a fitted ellipse to the particular contour. An ellipse is uniquely defined by a set of five parameters—the center of the ellipse ( $dxAvg, dyAvg$ ), its orientation ( $rotX$ ), and the lengths of its major and minor axes ( $aX, aY$ ) [23]. Here, the terms in the parenthesis are the abbreviations used in this paper (see Figure 9).

Due to the nonuniform shapes of the contours, the ellipse fitting is imperfect and introduces some approximation error. By representing the parameters using floating point values, the approximations made have more precision than if integer values were used. To further motivate the need for floating point numbers, the Match block uses these approximations to classify each ellipse as a head, torso, or hand. To do so, the relative locations, sizes, and other parameters are processed to within some hard-coded tolerances for classification. As an example, the algorithm considers two ellipses within a distance  $Y$  of each other with one being around  $X$  times larger than the other to be classified as a head/torso pair. It is because of the approximations and tolerances used by the algorithm that floating-point representations are desirable, as they allow the algorithm to operate with imperfect information and still produce reasonable results.

For our implementation, we used the IEEE 1076.3 Working Group floating-point packages, which are free and easily available from [24]. These packages have been under development for some time, have been tested by the IEEE Working Group, and are on a fast track to becoming IEEE standards. Efficient synthesis of floating point packages involved the evaluation of floating-point precision required by the smart camera algorithm. The C code version of the algorithm utilizes variables of type `double`, which represent 64-bit floating-point numbers. Utilizing the floating-point library mentioned before, we were able to vary the size of the floating-point numbers to see how the loss in precision affected the algorithm outputs as well as the area of the resulting synthesized design.

We reduced the number of bits used in the floating-point number representation and performed a series of simulations to determine the loss in accuracy relative to the original 64-bit algorithm. Figure 9 shows the resulting root-mean-square (RMS) error for various sizes of floating-point numbers. For the smart camera algorithm, we found that the range from 20- to 18-bit floating-point number representations gave sufficient accuracy, and any lower precision (such as 16-bit) caused a dramatic increase in the errors. The values that are most affected by the loss in precision are  $rotX$ ,  $aX$ , and to

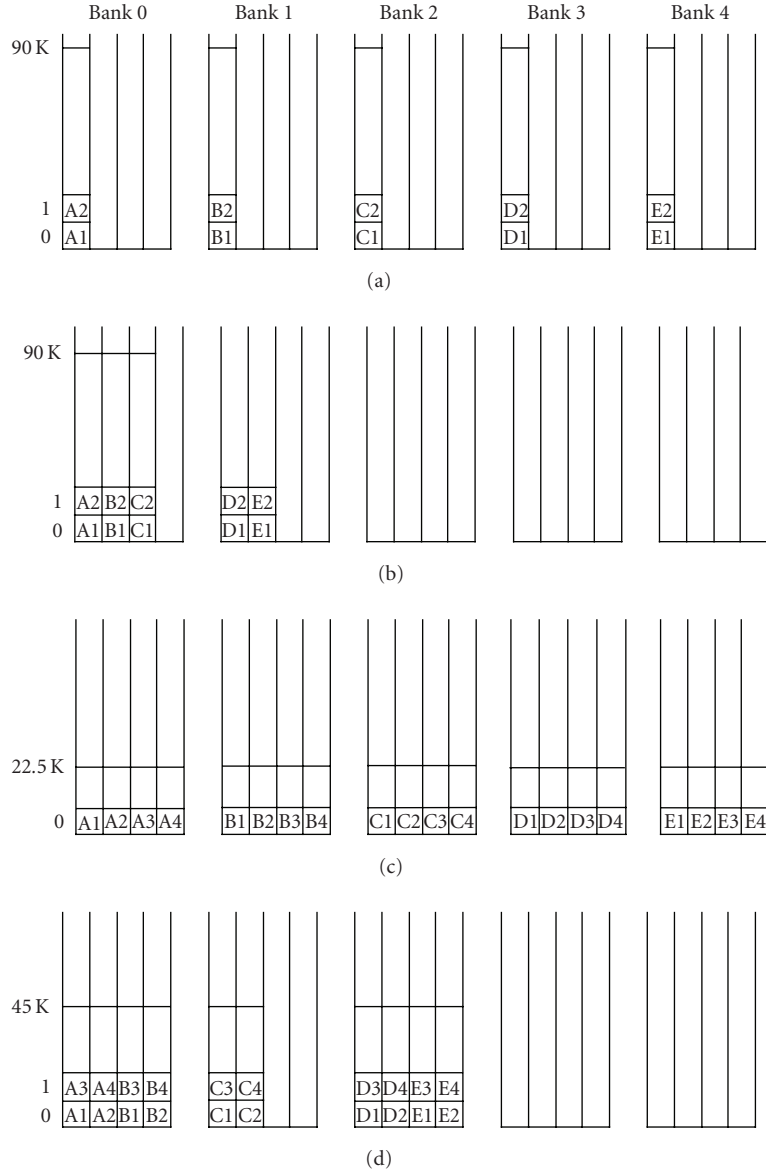


FIGURE 8: Image storage distribution. (a) Case 1: each image in a separate bank using only the first byte of the first 90 k words of the memory. (b) Case 2: three images in bank 0 and two in bank. (c) Case 3: each image in a separate bank but all four bytes used in each word, using 22.5 k words. (d) Case 4: images stored in three banks, each using 2 bytes of the first 45 k words.

some extent  $aY$ . These values depend on the computation of the *arctangent* function. As the precision is lowered, small variations cause large changes in the output of *arctangent*. The  $dxAvg$  and  $dyAvg$  parameters are not as affected by the loss in precision, as the only computations they require are addition and division.

Since the *arctangent* and *sqr*t functions have domains from  $\infty$  to  $-\infty$ , and *sqr*t also has a range of  $\infty$  to  $-\infty$ , theoretically the need might arise for expressing the whole real data set. The input image data set on which our experiment was performed was relatively small, and no prior knowledge was available of the range of values needed to be expressed for a new data set that the algorithm might be subjected to.

Thus our choice of floating point over fixed point for implementation and simulations was motivated by the lack of a quantization error metric and lack of predictability of the input data set for the low-level processing of the gesture recognition algorithm. Also this low-level processing is a precursor to higher-level gesture recognition algorithms for which, to our knowledge, no prior metric has been investigated to determine how errors in low-level processing effect the ability of the higher-level processing to correctly detect and process gestures. Through further simulation and analysis it may be possible to also determine suitable fixed-point precisions, however, care must be taken to ensure reliable results especially for the *arctangent* function.

TABLE 1: Comparison of different memory layout strategies.

Configuration	Banks used	Read cycles- Region	Write cycles- Region	Read cycles- Contour	Total non- overlapping cycles	Total number of cycles
Case1	5	92160X3	92160X2	184320X1	276480	645120
Case2	2	92160X1	92160X1	184320X1	276480	368640
Case3	5	23040X3	23040X2	46080X1	69120	161280
Case4	3	46080X2	46080X1	92160X1	138240	230400

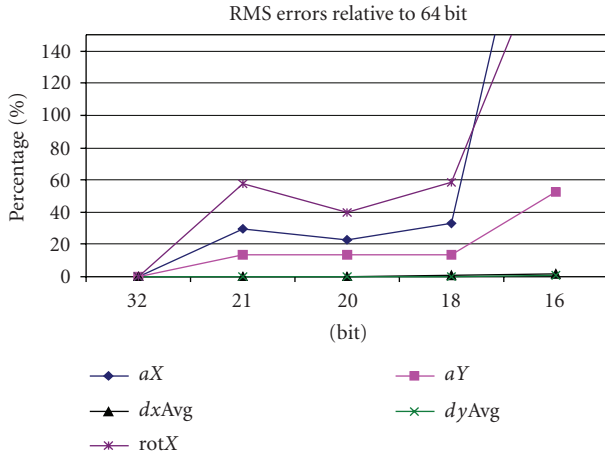


FIGURE 9: Comparison of percentages RMS error for different-length floating point of representations, normalized to a 64-bit floating-point representation.

TABLE 2: Synthesis results.

Number of bits	Area (in LUTs)
32-bit	110092
21-bit	54944
20-bit	46951
18-bit	41088
16-bit	23923

Table 2 presents the area in number of look-up tables required for each of the floating-point number representations. As expected, when we reduce the number of bits, the area of the resulting design decreases, but at the cost of lost precision.

The number of available LUTs in an FPGA varies heavily depending on the family of the FPGA and also on the specific devices within the family. For example, in the Virtex II family of the Xilinx FPGAs, the XC2V1000 contains 10,240 LUTs, the XC2V2000 contains 21,504 LUTs, and the XC2V8000 contains 93,184 LUTs. In the Xilinx Virtex II Pro family, the XC2VP7 contains 9,856 LUTs and XC2VP100 contains 88,192 LUTs (other intermediate devices in the family are omitted). In our experimental setup, we used the XC2V2000 FPGA, which did not have enough resources for us to implement Ellipse with the desired precision on the board (our

current implementation involves 16-bit floating point numbers and additional optimizations) but a larger FPGA would have sufficed.

## 9. RESULTS

In this section, we present some representative results from both software and hardware implementations of the gesture recognition algorithm.

We developed a software implementation of the gesture recognition algorithm on a Texas Instruments (TI) programmable digital signal processor. We evaluated this implementation using the TI Code Composer Studio version 2 for the C6xxx family of programmable DSP processors. The application, when implemented with our HPDF model, for a C64xx fixed-point DSP processor has a runtime of 21405671 cycles, and with a clock period of 40 nanoseconds, the execution time was calculated to be 0.86 second. The scheduling overhead for the implementation is minimal, as the HPDF representation inherently leads to a highly streamlined quasistatic schedule. The worst-case buffer size for an image of  $348 \times 240$  pixels was 184 kilobytes on the edge between Region and Contour, 642 Kb between Contour and Ellipse, and 34 Kb between Ellipse and Match for a total of 860 kilobytes. The original code (without modeling) had a run-time of 27741882 cycles, and with the same clock period of 40 nanoseconds, the execution time was 1.11 seconds. Thus, HPDF-based implementation improved the execution time by 23 percent.

To further take advantage of the parallelism exposed by HPDF modeling, we implemented both the Region and Contour functions in hardware. We used ModelSim XE II 5.8c for HDL simulation, Synplify Pro 7.7.1 for synthesis of the floating-point modules, and Xilinx ISE 6.2 for synthesis of nonfloating-point modules, and for downloading the bit-stream into the FPGA. Figures 10, 11, and 12 show the outputs of the first two processing blocks (Region and Contour, resp.) after they were implemented in HDL. Comparing these outputs with the outputs of the software implementation verified the correctness of the HDL modules.

## 10. CONCLUSIONS

In this paper, we have developed homogeneous parameterized dataflow (HPDF), an efficient metamodeling technique for capturing a commonly occurring restricted form of dynamic dataflow that is especially relevant to the computer vision domain. HPDF captures the inherent dataflow structure

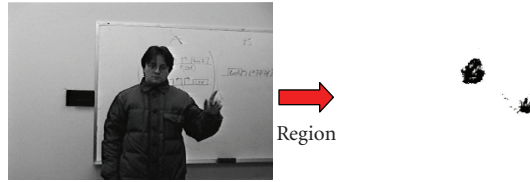


FIGURE 10: Our HDL representation of Region transforms the image on the left to the output of the right.

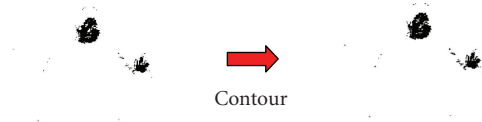


FIGURE 11: Actual transformation to the image done by HDL representation of Contour.

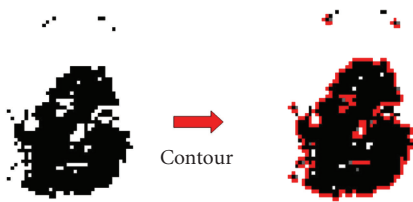


FIGURE 12: Part of Figure 10 zoomed-in and colored to show the effect of Contour.

in such applications without going into more complicated hierarchical representations or into more general dynamic dataflow modeling approaches where key analysis and synthesis problems become impossible to solve exactly.

We have also developed and applied a novel design methodology for effective platform-specific FPGA implementation of computer vision applications based on the HPDF modeling technique. In particular, we have used HPDF to model a gesture recognition algorithm that exhibits dynamically varying data production and consumption rates between certain pairs of key functional components.

The top-level HPDF model and subsequent intermediate representations that we derived from this model naturally suggested efficient hardware architectures for implementation of the main subsystems. The hardware description language (HDL) code for the four modules of the algorithm was developed following these suggested architectures. The modules were then verified for correctness, and synthesized to target a multimedia board from Xilinx. Memory management and floating point handling also played a major role in our design process. We explored various tradeoffs in these dimensions and through the framework of our HPDF-based application representation, we integrated our findings seamlessly with the architectural decisions described above.

## ACKNOWLEDGMENTS

This research was supported by Grant no. 0325119 from the US National Science Foundation. The multimedia board targeted in our experiments was donated by Xilinx, Inc.

## REFERENCES

- [1] S. Sriram and S. S. Bhattacharyya, *Embedded Multiprocessors: Scheduling and Synchronization*, Marcel Dekker, New York, NY, USA, 2000.
- [2] M. Sen, S. S. Bhattacharyya, T. Lv, and W. Wolf, "Modeling image processing systems with homogeneous parameterized dataflow graphs," in *Proceedings of IEEE International Conference on Acoustics, Speech and Signal Processing (ICASSP '05)*, vol. 5, pp. 133–136, Philadelphia, Pa, USA, March 2005.
- [3] S. S. Bhattacharyya, R. Leupers, and P. Marwedel, "Software synthesis and code generation for signal processing systems," *IEEE Transactions on Circuits and Systems II: Analog and Digital Signal Processing*, vol. 47, no. 9, pp. 849–875, 2000.
- [4] E. Lee and D. Messerschmitt, "Synchronous data flow," *Proceedings of the IEEE*, vol. 75, no. 9, pp. 55–64, 1987.
- [5] G. Bilsen, M. Engels, R. Lauwereins, and J. Peperstraete, "Cyclo-static dataflow," *IEEE Transactions on Signal Processing*, vol. 44, no. 2, pp. 397–408, 1996.
- [6] J. T. Buck, "A dynamic dataflow model suitable for efficient mixed hardware and software implementations of DSP applications," in *Proceedings of the 3rd International Workshop on Hardware/Software Codesign (CODES '94)*, pp. 165–172, Grenoble, France, September 1994.
- [7] B. Bhattacharya and S. S. Bhattacharyya, "Parameterized dataflow modeling for DSP systems," *IEEE Transactions on Signal Processing*, vol. 49, no. 10, pp. 2408–2421, 2001.
- [8] M. Gokhale, J. Stone, J. Arnold, and M. Kalinowski, "Stream-oriented FPGA computing in the Streams-C high level language," in *Proceedings of IEEE Symposium on Field-Programmable Custom Computing Machines*, pp. 49–56, Napa Valley, Calif, USA, April 2000.
- [9] C. A. R. Hoare, *Communicating Sequential Processes*, Prentice-Hall, New York, NY, USA, 1985.
- [10] S. Chappell and C. Sullivan, "Handel-C for co-processing & co-design of Field Programmable System on Chip," White Paper, Celoxica, Oxford, UK, September 2002.
- [11] P. Banerjee, D. Bagchi, M. Haldar, A. Nayak, V. Kim, and R. Uribe, "Automatic conversion of floating-point MATLAB programs into fixed-point FPGA based hardware design," in *Proceedings of the 41st Annual Design Automation Conference (DAC '04)*, pp. 484–487, San Diego, Calif, USA, June 2004.
- [12] B. Kienhuis, E. Rijpkema, and E. Deprattere, "Compaan: deriving process networks from Matlab for embedded signal processing architectures," in *Proceedings of the 18th International Workshop on Hardware/Software Codesign (CODES '00)*, pp. 13–17, San Diego, Calif, USA, May 2000.
- [13] G. Kahn, "The semantics of simple language for parallel programming," in *Proceedings of IFIP Congress*, pp. 471–475, Stockholm, Sweden, August 1974.
- [14] E. A. Lee, "Multidimensional streams rooted in dataflow," in *Proceedings of the IFIP Working Conference on Architectures and Compilation Techniques for Fine and Medium Grain Parallelism*, no. 23, pp. 295–306, Orlando, Fla, USA, January 1993.
- [15] W. Wolf, B. Ozer, and T. Lv, "Smart cameras as embedded systems," *Computer*, vol. 35, no. 9, pp. 48–53, 2002.
- [16] J. Eker, J. W. Janneck, E. A. Lee, et al., "Taming heterogeneity—the ptolemy approach," *Proceedings of the IEEE*, vol. 91, no. 1, pp. 127–144, 2003.

- [17] F. Haim, M. Sen, D.-I. Ko, S. S. Bhattacharyya, and W. Wolf, "Mapping multimedia applications onto configurable hardware with parameterized cyclo-static dataflow graphs," in *Proceedings of IEEE International Conference on Acoustics, Speech and Signal Processing (ICASSP '06)*, vol. 3, pp. 1052–1055, Toulouse, France, May 2006.
- [18] J. Horstmannshoff, T. Grötter, and H. Meyr, "Mapping multirate dataflow to complex RT level hardware models," in *Proceedings of the International Conference on Application-Specific Systems, Architectures and Processors (ASAP '97)*, pp. 283–292, Zurich, Switzerland, July 1997.
- [19] M. Sen and S. S. Bhattacharyya, "Systematic exploitation of data parallelism in hardware synthesis of DSP applications," in *Proceedings of IEEE International Conference on Acoustics, Speech and Signal Processing (ICASSP '04)*, vol. 5, pp. 229–232, Montreal, Quebec, Canada, May 2004.
- [20] M. C. Williamson and E. A. Lee, "Synthesis of parallel hardware implementations from synchronous dataflow graph specifications," in *Proceedings of the 30th Asilomar Conference on Signals, Systems and Computers*, vol. 2, pp. 1340–1343, Grove, Calif, USA, November 1996.
- [21] Data-sheet for ZBT memory, <http://www.samsung.com/Products/>.
- [22] OpenCores Organization, "WISHBONE System-on-Chip (SoC) Interconnection Architecture for Portable IP Cores," revision B.3, September 2002, <http://www.opencores.org>.
- [23] A. K. Jain, *Fundamentals of Digital Image Processing*, Prentice-Hall, New York, NY, USA, 1989.
- [24] IEEE Working Group, <http://www.eda.org/vhdl-200x/vhdl-200x-ft/packages/files.html>.